

Lens Distortion Effects on CMB Maps

F. Bernardeau

Service de Physique Théorique, C.E. de Saclay, F-91191 Gif-sur-Yvette cedex, France

October 29, 2018

Abstract. Weak lensing effects are known to introduce non-linear couplings in the CMB temperature maps. In inflationary scenario, the primary CMB anisotropies are expected to form a 2D Gaussian map, for which, the probability distribution function of the ellipticity defined from the local temperature curvature matrix has a very specific shape. I show that lenses alter significantly the shape of this PDF, inducing an excess of elongated structures. The precise functional form is computed for both the field points and the temperature extrema.

These analytical results are confirmed by numerical experiments on 10x10 square degree maps. These numerical results allow to investigate the effects of smoothing and to estimate the cosmic variance. For the best resolution and sky coverage of the Planck mission the signal to noise ratio for the statistical indicators presented here is about 3 to 6 depending on the cosmological models. A marginal detection should therefore be possible.

Key words: Cosmology: Dark Matter, Large-Scale Structures, Gravitational Lensing, Cosmic Microwave Background

1. Introduction

The detection by the COBE/DMR experiment (Smoot et al. 1993) of the anisotropies of the CMB temperature at very large angular scales, above 7 deg, has open an exiting new mean of investigation for cosmology. Many experiments that are now under development will provide us in the near future with precious data at smaller angular scale, down to a fraction of a degree. At such angular scales the dominant mechanism that generates the CMB anisotropies is the primary, linear order, coupling of the various cosmic fluids (photons, baryons and different species of possible dark matter) before and during recombinaison. Whether the primary anisotropies originate

from quantum fluctuations in an inflationary scenario, or from other mechanisms such as topological defects generated in a phase transition epoch is yet unclear. This is undoubtedly a major scientific goal for the coming experiments. Indeed, one of the clearest signature of the topological models is that they are expected to induce non-Gaussian primary temperature fluctuations (Pen et al. 1994, Turok 1996, Barnes & Turok 1996). But even in the case of inflationary scenario, it is possible that secondary effects, non-linear couplings of the radiation field with matter, induce non-Gaussian features. This is particularly important at very small angular scale, down to the arcmin scale. I am more particularly interested here in the static lens effects. The effects of the gravitational distortion on the power spectrum of the primary temperature maps have been the subject of many investigations in the last decade (Blanchard & Schneider 1987, Kashlinsky 1988, Cole & Efstathiou 1989, Sasaki 1989, Tomita & Watanabe 1989, Linder 1990, Cayón, Martínez-González & Sanz 1993a, b, Fukushige, Makino & Ebisuzaki 1994, Seljak 1996). It is now clear that the lens effect on the power spectrum is small, although it is probably worth to take it into account in a very detailed analysis of such measurements. In principle, for an inflationary scenario, a detailed analysis of the CMB power spectrum should allow to constrain very accurately the cosmological parameters (see for instance Jungman et al. 1996). But it would be anyway extremely interesting to be able to have a positive detection of the lens effect since it can potentially be used to constrain the amplitude of the cosmic density power spectrum, independently of the constraints obtained from the CMB power spectrum itself. It could therefore be a precious test for the cosmological model(s) favored by the shape of the CMB power spectrum.

In a previous paper, the four point functions induced by the lens effects has been investigated (Bernardeau 1997). This is the most direct quantity that can be calculated from the coupling terms introduced by the lenses. One thus obtains specific properties of CMB maps induced by the lenses. Another possible way of investigation is to look for cross-correlation between the CMB temperature

Send offprint requests to: F. Bernardeau; fbernardeau@cea.fr

gradients and the displacement field induced by the projected large-scale structures (Suginohara et al. 1997). The signal however depends on the bias properties of the galaxies. It cannot be directly interpreted in terms of cosmological parameters.

If the four point function is indeed sensitive to the intrinsic depth of the lens potential wells, it is not necessarily the best indicator in terms of signal to noise ratio for a realistic experiment. The aim of this paper is therefore to investigate new means of detecting these effects. In section 2 I present numerical results showing peculiar examples of the lens effects on temperature maps. The visual impression is that the lens effects induce a change in the topological properties of the temperature maps, and not so much in the local temperature distribution function.

This is the motivation for the investigation of other statistical indicators that can reveal the lens effects with a better efficiency. Particularly interesting can be the statistical properties of the local curvature of the temperature maps. The matrix of the second order temperature derivatives has indeed specific statistical properties in case of a 2D Gaussian field. These properties are affected when the lens effects are taken into account because of the induced mode couplings. More specifically a quantity that can be a good tracer of the lens effect is the probability distribution function of the local ellipticity since lenses tend to systematically stretch the local temperature patches. Compared to the 4-point function the motivation for considering such a quantity is then double. First of all, the cosmic variance is expected to be smaller: It is given by statistical properties related to the second order derivative, and therefore more sensitive to the small scale temperature fluctuations. Secondly the effects of lenses on the four-point function were found to be proportional to the cosine of the angle joining the observational directions (see Bernardeau 1997), which tends to substantially reduce the lens signal when it is averaged for the computation of the four point moment. Such a cancellation is not expected for the distortion effect on the curvature. The derivation of the lens effect for the distribution function of the local ellipticity is presented in Section 3. In Section 4, results are confronted with numerical experiments. In particular I estimate the cosmic variance for the ellipticity statistics. In the last section I discuss the dependence of the lens effects on the cosmological parameters.

2. The physical mechanisms

First of all let me recall the basic effect induced by the lenses. I am interested here in the static lenses caused by the presence along the line-of-sights of large-scale concentrations of matter. These concentrations of matter are of course intrinsic to any theory of large-scale structure formation. The effects presented in this paper are therefore robust consequences of the growth of structures. The amplitude of the effects, however, depends not only on the

amplitude of the local fluctuations but also on the global cosmological parameters: the lens effects are all the more large that the CMB plane is distant from the lenses. The dependence of the signal on the cosmological parameters is discussed in the last section. The static lenses (contrary to the case of moving lenses, see Birkinshaw & Gull 1983) do not change the background temperature of the CMB, but only induce a displacement field so that the observed temperature fluctuation in a given direction γ is the one coming from a slightly shifted direction, $\gamma + \xi(\gamma)$,

$$\delta_T^{\text{obs.}}(\gamma) = \delta_T^{\text{prim.}}(\gamma + \xi(\gamma)), \quad (1)$$

where $\xi(\gamma)$ is the displacement field induced by the lenses along the line of sight in the direction γ . Written in terms of the gravitational potential Ψ , the displacement reads,

$$\xi(\gamma) = -2 \int_0^{\chi_{\text{CMB}}} d\chi \frac{\mathcal{D}(\chi_{\text{CMB}}, \chi)}{\mathcal{D}(\chi_{\text{CMB}})} \nabla \psi(\gamma, \chi), \quad (2)$$

where χ and \mathcal{D} are respectively the radial and angular distances. These quantities are identical in case of a background universe with zero curvature. \mathcal{D}_{CMB} is the angular distance to the last scattering surface. The lens population identifies with the large-scale structures of the Universe that are present along the line of sights. It is important to have in mind that the displacements induced by these matter concentrations are at most of the order of 1 arcmin for cluster cores, whereas the instrumental resolution for the future satellite missions¹ is at best 5 arcmin. As a result, it is safe to neglect the influence of the critical regions and the lens effect is assumed here to be fully in the weak lensing regime.

A consequence of this remark is that the effects investigated in this paper can be entirely described by the two-point correlation properties of the lens population. The precise reason is that the displacement field being a small perturbation of the primordial field, its leading contribution can be expressed perturbatively solely with the two-point correlation function of either the displacement field or its derivatives such as the local gravitational convergence. This situation was already encountered in the computation of the induced temperature four-point function (Bernardeau 1997). Therefore, the lens effects will depend quantitatively only on the shape and magnitude of the cosmic density power spectrum, $P(k)$, defined from the Fourier transform of the local density field,

$$\delta(\mathbf{x}) = \int \frac{d^3\mathbf{k}}{(2\pi)^{3/2}} \delta_{\mathbf{k}} \exp(i\mathbf{k} \cdot \mathbf{x}), \quad (3)$$

with then,

$$\langle \delta_{\mathbf{k}} \delta_{\mathbf{k}'} \rangle = \delta_{\text{Dirac}}(\mathbf{k} + \mathbf{k}') P(k). \quad (4)$$

¹ Note however that ground based interferometer instruments can potentially reach a better resolution.

Note that in this analysis, $P(k)$, is the actual power spectrum, that includes possible nonlinear evolution of the density field. Written in terms of the modes $\delta_{\mathbf{k}}$ the displacement field reads,

$$\xi(\gamma) = \int_0^{\chi_{\text{CMB}}} d\chi w(\chi) \int \frac{d^3\mathbf{k}}{(2\pi)^{3/2}} \times \frac{i\mathbf{k}_\perp}{k^2 \mathcal{D}(\chi)} \delta(\mathbf{k}) \exp[i\mathcal{D}(\chi)\mathbf{k}_\perp \cdot \boldsymbol{\gamma} + ik_r \chi], \quad (5)$$

with,

$$w(\chi) = \frac{3\Omega_0}{a(\chi)} \frac{\mathcal{D}(\chi_{\text{CMB}} - \chi) \mathcal{D}(\chi)}{\mathcal{D}(\chi_{\text{CMB}})}. \quad (6)$$

The function $w(\chi)$ gives the lens efficiency function for sources located on the last scattering surface. The second moment of the displacement field then reads

$$\langle \xi^2 \rangle = \int_0^{\chi_{\text{CMB}}} d\chi w(\chi) \int_0^{\chi_{\text{CMB}}} d\chi' w(\chi') \int \frac{d^3\mathbf{k}}{(2\pi)^3} \times P(k) \frac{\mathbf{k}_\perp^2}{k^4 \mathcal{D}^2} \exp[i(\mathcal{D}(\chi) - \mathcal{D}(\chi'))\mathbf{k}_\perp \cdot \boldsymbol{\gamma} + ik_r(\chi - \chi')]. \quad (7)$$

Applying the small angle approximation, the integral in k_r introduces a Dirac function in $\chi = \chi'$ so that

$$\langle \xi^2 \rangle = \int_0^{\chi_{\text{CMB}}} d\chi w^2(\chi) \int \frac{d^2\mathbf{k}}{(2\pi)^2} \frac{P(k)}{k^2 \mathcal{D}^2}. \quad (8)$$

It is then simple to see that the displacement field can be expressed in terms of a 2d projected potential, p_{2d} , defined by

$$p_{2d}(l) = \int_0^{\chi_{\text{CMB}}} d\chi \frac{w^2(\chi)}{\mathcal{D}^2} P[l/\mathcal{D}(\chi)], \quad (9)$$

with

$$\langle \xi^2 \rangle = \int \frac{d^2\mathbf{l}}{(2\pi)^2} \frac{p_{2d}(l)}{l^2}. \quad (10)$$

The lens effects are thus entirely determined by p_{2d} .

2.1. Numerical Experiments

The effect of the mechanism described in (1) can be easily visualized in a simple numerical experiment. A realistic temperature map can be generated from a given power spectrum, C_l . A 2D displacement field can also be generated as a realization of a Gaussian process with the power spectrum p_{2d} obtained from a given 3D power spectrum. In the following I use a standard CDM model for both the temperature map and the displacement field. The normalization of the temperature power spectrum is arbitrary; the one of the displacement field will be discussed in terms of σ_8 , i.e. the r.m.s. of the density fluctuations at $8h^{-1}$ Mpc scale. A technical simplification is to assume that the displacement field is Gaussian. This is obviously

not exact, specially at small scale, but as it has already been mentioned, the lens effects depend only on the power spectrum of the projected lens density. To mimic the effects of the lens on the CMB maps it is thus not necessary to have a full 3D realization of the large-scale structures. Note that the non-linear effects for the evolution of the lens density field are implicitly taken into account with the use of the non-linear power spectrum $P(k)$ (Jain et al. 1995, Peacock & Dodds 1996, following the approach of Hamilton et al. 1991). The effects of the lenses are then computed from the equation (1): it means that the lensed temperature map is given by the primordial one, but on a now irregular grid. The lensed temperature map is obtained by a ‘‘regridding’’ of the temperature map, with a local linear interpolation of the temperature with the nearest neighbors. This algorithm is usually available in standard mathematical packages.

The two maps of Fig 1 show the effects of lenses. The effect is of course magnified so that it can be easily detected by a visual inspection of a very small map. The value of σ_8 would be here of about 2. The size of the maps is 4x4 degrees, for a pixel size of 1.17'. On the lensed map, one can see that the temperature patches are still present with the same temperature contrasts. They are however displaced and deformed. The most striking feature is probably that there are very sharp edges and extended area of constant gradients. All these features suggest that the local curvature is probably a good indicator of the lens effects.

3. The lens effects on the local temperature curvature

3.1. The local curvature for the primordial temperature map

The temperature curvature is defined from the matrix of the second order derivatives of the local temperature,

$$c_{ij} \equiv \frac{d^2 \delta_T}{dx_i dx_j} \quad (11)$$

that can be written,

$$c_{ij} = \begin{pmatrix} \frac{d^2 \delta_T}{(dx_1)^2} & \frac{d^2 \delta_T}{dx_1 dx_2} \\ \frac{d^2 \delta_T}{dx_1 dx_2} & \frac{d^2 \delta_T}{(dx_2)^2} \end{pmatrix} \equiv \begin{pmatrix} \tau + g_1 & g_2 \\ g_2 & \tau - g_1 \end{pmatrix}. \quad (12)$$

The previous equation defines the scalar field τ and the vector field \mathbf{g} . Note that a rotation of the coordinate system with an angle θ transforms the components of c_{ij} in

$$\begin{aligned} \tau' &\rightarrow \tau, \\ \mathbf{g}' &\rightarrow \mathcal{R}_{2\theta} \cdot \mathbf{g}, \end{aligned} \quad (13)$$

where $\mathcal{R}_{2\theta}$ is the rotation matrix of angle 2θ . Thus the vector \mathbf{g} behaves rather like a pseudo-vector. For a Gaussian temperature field it is easy to show that τ , g_1 and

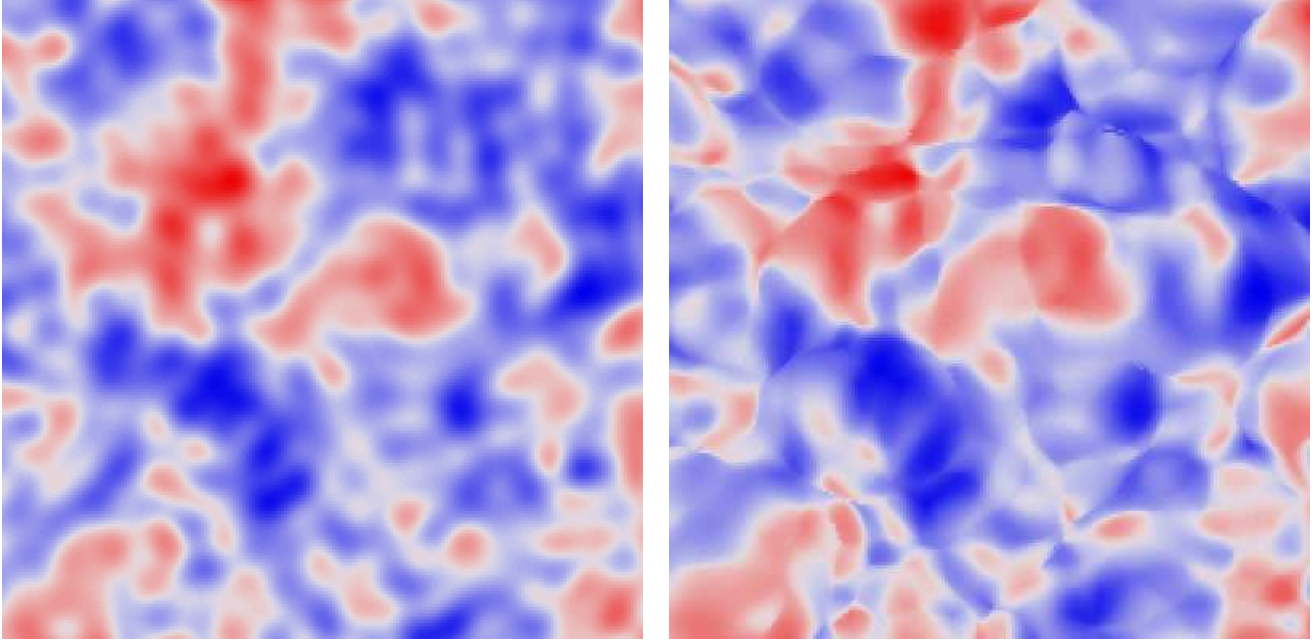


Fig. 1. An example of primordial temperature map (left) deformed by the lens effect (right). It corresponds to a CDM model. The figures are 4×4 square degree large. The lensed effects have been magnified to make them visible. The displacement field has been multiplied by about 4.

g_2 are three Gaussian *independent* fields. At a given point their variances are given by,

$$\langle \tau^2 \rangle = \sigma_2^2, \quad (14)$$

$$\langle g_1^2 \rangle = \langle g_2^2 \rangle = \frac{1}{2} \sigma_2^2, \quad (15)$$

with σ_2 given, in the small angle approximation, by

$$\sigma_2^2 = \frac{1}{4} \int \frac{d^2 l}{(2\pi)^2} l^4 C_l, \quad (16)$$

where C_l is the temperature power spectrum. This entirely defines the statistical properties of the quantities associated with the primordial temperature field.

A quantity of interest is then the ellipticity,

$$e = \frac{g}{2\tau}, \quad (17)$$

where g is naturally given by,

$$g = \sqrt{g_1^2 + g_2^2}. \quad (18)$$

The local ellipticity expresses the fact the temperature fluctuations may be locally isotropic or not. Let me be a bit more precise. First of all it is always possible to assume that g_2 equals zero (by a proper choice of coordinates) so that $g = |g_1|$. Consider then the curvature matrix c_{ij} and

its 2 eigenvalues. They identify with $\tau - g$ and $\tau + g$. If they have the same sign, as it is the case for a local extremum, it is also the sign of τ and consequently the one of the ellipticity. In such a case, when the ellipticity is positive, $\tau - g$ is positive and the ellipticity is smaller than $1/2$. In general the absolute value of extremum ellipticities is less than $1/2$, i.e. elongated peaks correspond to ellipticities close to $1/2$ and round structures close to 0 whereas values larger than $1/2$ correspond to regions of eigenvalues of different sign such as saddle points².

The distribution function of the local ellipticity can be easily computed from the known statistical properties of τ and g . One finds that (eg. Bond & Efstathiou 1987),

$$p_e^{\text{prim.}}(e)de = \frac{4|e|de}{(1+8e^2)^{3/2}}. \quad (19)$$

As there are no statistical differences at all between the hot and the cold regions in the primordial map, and since the lens effects do preserve this property, in the following I will consider only the cases of positive ellipticities. It is important to note that *the distribution (19) does not depend on the shape of the temperature power spectrum*. It is specific of a 2D Gaussian field.

² Note that although this discussion is focussed on points of vanishing temperature gradient, the curvature tensor and the local ellipticity are defined on every field point.

In (19) e runs from 0 to ∞ (when limited to a positive ellipticity). For practical reason I make the change of variable,

$$\epsilon = 1 / \left(\frac{1}{2e} + 1 \right) \quad (20)$$

so that ϵ runs from 0 to 1. The distribution of ϵ can be easily computed from the one in e ,

$$p_\epsilon^{\text{prim.}}(\epsilon)d\epsilon = \frac{2\epsilon d\epsilon}{(1 - 2\epsilon + 3\epsilon^2)^{3/2}}, \quad 0 \leq \epsilon \leq 1. \quad (21)$$

This distribution peaks at $\epsilon = 0.5$. The numerical results will be discussed in terms of ϵ because a binning of constant width is obviously more appropriate for ϵ compared to e .

The effect of lenses is, from the visual inspection of figure 1, to extend the regions with very asymmetric curvature, that is to favor regions of ellipticity close to 1/2. The aim of the coming sections is to quantify analytically this effect.

3.2. The lens effects

3.2.1. The lens effects on the curvature matrix

We have now to consider the local curvature matrix in the presence of lenses. The first derivative of eq. (1) leads to

$$(\delta_T^{\text{obs.}})_{,i} = (\delta_T^{\text{prim.}})_{,j}(\delta_{ji}^K + \xi_{j,i}) \quad (22)$$

where δ_{ij}^K is the Kronecker symbol. This expression makes naturally intervene the lens amplification matrix, \mathcal{A}_{ij} ,

$$\mathcal{A}_{ij} \equiv \text{Id} + (\xi_{i,j}) = \begin{pmatrix} 1 - \varphi_{,11} & -\varphi_{,12} \\ -\varphi_{,12} & 1 - \varphi_{,22} \end{pmatrix}, \quad (23)$$

where Id is the identity matrix and φ is the projected potential of the matter density fluctuations along the line-of-sight (the power spectrum of which obviously is $p_{2d}(l)/l^2$). Note that in the weak lensing regime the matrix \mathcal{A} is always regular, so that the extrema are conserved by the lens effects (at least as long as filtering is not taken into account).

The second order derivatives of eq. (1) lead to

$$(\delta_T^{\text{obs.}})_{,ij} = (\delta_T^{\text{prim.}})_{,kl}(\delta_{ki}^K + \xi_{k,i})(\delta_{lj}^K + \xi_{l,j}) + (\delta_T^{\text{prim.}})_{,k} \xi_{k,ij}. \quad (24)$$

Two terms appear. The second term vanishes for a peak, and in such a case the lens effect can be written in a rather compact way,

$$\mathcal{C}^{\text{obs.}} = \mathcal{A} \cdot \mathcal{C}^{\text{prim.}} \cdot \mathcal{A}, \quad (25)$$

where \mathcal{C} is the curvature matrix. This expression is familiar in studies of weak lensing effects on background galaxies. It is also interesting to note that a peak cannot be transformed in a saddle point, and inversely: from relation (25) it appears that the determinants of $\mathcal{C}^{\text{prim.}}$ and $\mathcal{C}^{\text{obs.}}$ have the same sign, as long as the lens effect is not critical.

3.2.2. The local ellipticity distribution

The computation of the statistical properties of the matrix element of the curvature matrix of the lensed map then requires the knowledge of the statistical properties of the lens contributions. First of all the displacement field is statistically independent of the temperature fluctuations of the CMB. Secondly the displacement is small, so that it is safe to do a perturbative calculation with respect to the displacement. It implies that only the second moment of the displacement, and of its derivatives, will appear in the final results.

The components of the amplification matrix \mathcal{A} can be written in terms of the local gravitational convergence κ and distortion γ ,

$$\mathcal{A} \equiv \begin{pmatrix} 1 - \kappa - \gamma_1 & -\gamma_2 \\ -\gamma_2 & 1 - \kappa - \gamma_1 \end{pmatrix}. \quad (26)$$

Similarly to the case of the curvature matrix the r.m.s. values of κ , γ_1 and γ_2 are related to each other through,

$$\langle \gamma_1^2 \rangle = \langle \gamma_2^2 \rangle = \frac{1}{2} \langle \kappa^2 \rangle \equiv \frac{1}{2} \sigma_\kappa^2, \quad (27)$$

although κ and γ_i may not be Gaussian distributed. This is a simple consequence of geometrical averages, that take advantage of the assumed statistical isotropy of the displacement field. The second moment of the local convergence, σ_κ^2 , is related to the projected power spectrum with³,

$$\sigma_\kappa^2 = \frac{1}{4} \int \frac{d^2\mathbf{l}}{(2\pi)^2} p_{2d}(l). \quad (28)$$

The relation between σ_κ and the normalization of the local density spectrum, σ_8 , makes intervene the projection effects that depend on the cosmological parameters. That will be discussed in more detail in the last section.

The second order derivatives are all independent of the first order derivatives. Only 4 different terms are generated, $\xi_{1,11}$, $\xi_{1,12}$, $\xi_{1,22}$ and $\xi_{2,22}$. The others are identical to one of those 4 because the displacement is potential. Then we have,

$$\begin{aligned} \langle \xi_{1,11}^2 \rangle &= 5/16 s^2, \\ \langle \xi_{2,22}^2 \rangle &= 5/16 s^2, \\ \langle \xi_{1,12}^2 \rangle &= 1/16 s^2, \\ \langle \xi_{1,22}^2 \rangle &= 1/16 s^2, \\ \langle \xi_{1,11} \xi_{1,22} \rangle &= 1/16 s^2, \\ \langle \xi_{1,12} \xi_{2,22} \rangle &= 1/16 s^2, \end{aligned} \quad (29)$$

and the other cross-correlation terms are zero. This is again a simple consequence of geometrical averages. The quantity s is also related to the projected power spectrum,

$$s^2 = \int \frac{d^2\mathbf{l}}{(2\pi)^2} l^4 p_{2d}(l). \quad (30)$$

³ This expression ignores the effects of filtering and is thus not realistic. I reconsider this at the end of this section.

The calculation of the statistical properties of the curvature elements is then now quite straightforward. One has to (perturbatively) invert the relation between the quantities associated with the lensed map and the primordial map, and then to compute the distribution function τ and g_i from their distribution function in the unlensed case. These calculations are in practice a bit lengthy but can be performed without much difficulty with a formal calculator. One then has,

$$p^{\text{obs.}}(\tau, g_1, g_2) = p^{\text{prim.}}(\tau, g_1, g_2) [1 + Q_1 \sigma_\kappa^2 + Q_2 s^2], \quad (31)$$

with

$$Q_1 = -24 + 24\tau^2 - 2\tau^4 + 39g^2 - 17\tau^2 g^2 - 8g^4, \quad (32)$$

$$Q_2 = (-3 + \tau^2 + 2g^2)/8. \quad (33)$$

From these expressions it is easy to compute the new distribution function for the ellipticity,

$$p_e^{\text{obs.}}(e) = p_e^{\text{prim.}}(e) \left[1 + \sigma_\kappa^2 \frac{18(-1 + 20e^2 - 16e^4)}{(1 + 8e^2)^2} \right]. \quad (34)$$

Remarkably the term in s^2 disappears. The relation (34) is one of the central results of this paper. In the following this result is compared with results of numerical experiments.

3.3. The extrema ellipticity distribution

3.3.1. For a Gaussian field

The calculation of the ellipticity of the extrema has been examined in detail by Bond & Efstathiou (1987) in case of a 2D Gaussian field. The principle of the calculation relies on the computations of the number of peaks, $N_{\text{peak}}(\tau, \mathbf{g})$ of a given curvature (within the range $d\tau$ and $d^2\mathbf{g}$). If the extrema have the directions γ_p in a given sample then,

$$N_{\text{peak}}(\tau, \mathbf{g}) d\tau d^2\mathbf{g} = \int d^2\gamma \sum_p \delta_{\text{Dirac}}(\gamma - \gamma_p) \text{Pr.}(\tau, \mathbf{g} | \nabla \delta_T = 0) d\tau d^2\mathbf{g}, \quad (35)$$

where $\text{Pr.}(\tau, \mathbf{g} | \nabla \delta_T = 0)$ is the probability distribution function of the local curvature under the constraint that the local gradient vanishes. In case of a Gaussian field this expression simplifies since the local gradients are statistically independent of the curvature, i.e.,

$$\text{Pr.}^{\text{prim.}}(\tau, \mathbf{g} | \nabla \delta_T^{\text{prim.}} = 0) = \text{Pr.}^{\text{prim.}}(\tau, \mathbf{g}). \quad (36)$$

The trick to complete the calculation is then to express the Dirac delta functions in $\gamma - \gamma_p$ in terms of the local curvature. Indeed, for peaks we can Taylor expand the local temperature gradient in,

$$(\delta_T)_{,i}(\gamma) = (\delta_T)_{,ji}(\gamma_p)(\gamma - \gamma_p)_j, \quad (37)$$

since, by definition, $(\delta_T)_{,i}(\gamma_p) = 0$. As a result we have for the primordial field,

$$N_{\text{peak}}(\tau, \mathbf{g}) d\tau d^2\mathbf{g} = N_{\text{tot.}} \frac{J(\tau, \mathbf{g}) \text{Pr.}(\tau, \mathbf{g}) d\tau d^2\mathbf{g}}{\int J(\tau, \mathbf{g}) \text{Pr.}(\tau, \mathbf{g}) d\tau d^2\mathbf{g}}, \quad (38)$$

where $N_{\text{tot.}}$ is the total number of peaks, and $J(\tau, \mathbf{g})$ is the Jacobian of the transform between the positions and the gradients, i.e.,

$$J(\tau, \mathbf{g}) = |\text{Det}(c_{ij})| = |\tau^2 - \mathbf{g}^2|. \quad (39)$$

As a result we have,

$$n_{\text{peak}}^{\text{prim.}}(\tau, \mathbf{g}) d\tau d^2\mathbf{g} = \frac{|\tau^2 - \mathbf{g}^2| p^{\text{prim.}}(\tau, \mathbf{g}) d\tau d^2\mathbf{g}}{\int |\tau^2 - \mathbf{g}^2| p^{\text{prim.}}(\tau, \mathbf{g}) d\tau d^2\mathbf{g}}, \quad (40)$$

which, after simple calculations, implies that,

$$p_{\text{peak}}^{\text{prim.}}(e) de = \frac{24 \sqrt{3} (1 - 4e^2) e de}{(1 + 8e^2)^{5/2}}, \quad (41)$$

when the integration is limited to the maxima (extrema with positive curvature), that is when $\tau^2 > g^2$ and $\tau > 0$.

3.3.2. The peak ellipticity distribution with lens effects

In this section I investigate the effects of lenses for the ellipticity distribution of the extrema. The principle of the calculation is very similar derivation to the Gaussian field case. The only change is that in principle the local curvature may not be independent of the gradient. Actually for peaks we know that (25) is exact so that we can express the curvature of the lensed map in terms of the curvature of the primordial map for which the statistical properties are completely defined. The effect of lenses will then show up in the distribution function of the local curvature and in the expression of the Jacobian. Taking these two changes into account we have,

$$p_{\text{peaks}}^{\text{obs.}}(\tau, g_1, g_2) = p_{\text{peaks}}^{\text{prim.}}(\tau, g_1, g_2) [1 + Q_3 \sigma_\kappa^2], \quad (42)$$

with

$$Q_3 = -28 + 24\tau^2 + 39g^2 - 2\tau^4 - 17\tau^2 g^2 - 8g^4. \quad (43)$$

Note that in this case it is necessary to make sure that the integral is correctly normalized. The number density of peaks remain unchanged with (sub-critical) lenses but the variances for the curvature or the gradient are perturbatively affected. From the previous result we have,

$$p_{\text{pk}}^{\text{obs.}}(e) = p_{\text{pk}}^{\text{prim.}}(e) \left[1 + \frac{2(-15 + 512e^2 - 112e^4)}{(1 + 8e^2)} \sigma_\kappa^2 \right]. \quad (44)$$

A straightforward examination of (34) and (44) show that the effect of lens distortion is significantly larger for the peaks compared to the field points.

3.4. The effects of filtering

So far, in these analysis, I have ignored the effects of filtering. Actually the CMB temperature maps will be observed with a finite resolution. The measured temperature map is thus given by

$$\tilde{\delta}_T(\gamma) = \int d^2\gamma' W(|\gamma - \gamma'|/\theta_0) \delta_T(\gamma'), \quad (45)$$

where W is a window function that in practice can be assumed to be Gaussian. It is anyway possible to further filter the resulting maps. In particular it can be very interesting to filter the large angular scale modes out in order to reduce the cosmic variance. In all cases, the filtered lensed temperature map is given by

$$\tilde{\delta}_T^{\text{obs.}}(\gamma) = \int d^2\gamma' W(|\gamma - \gamma'|/\theta_0) \delta_T^{\text{prim.}}(\gamma' + \xi(\gamma')). \quad (46)$$

It is obviously not equivalent to the lens distortion effects applied to the filtered primordial temperature map! The two operations do not commute in general. This is a standard problem when one is considering the effects of non-linear couplings. In this particular problem there is however a limiting case for which the problem can be completely solved. Indeed the CMB temperature maps has an intrinsic small-scale cutoff due to the Silk damping effect. If then the filtering scale is much smaller than this intrinsic scale one can assume that locally $\delta_T^{\text{prim.}}(\gamma') \approx \delta_T^{\text{prim.}}(\gamma)$ when γ' is close enough to γ . As a result we have

$$(\tilde{\delta}_T^{\text{obs.}})_{,i}(\gamma) \approx (\delta_T^{\text{prim.}})_{,j} \times [\delta_{ji}^K + \int d^2\gamma' W(|\gamma - \gamma'|/\theta_0) \xi(\gamma')_{j,i}]. \quad (47)$$

The filtering effect applies only to the displacement field. The same situation occurs for the 2nd order derivatives. In this limiting case, the effect of filtering is then simply to reduce the lens effect by filtering the displacement field. It implies in particular that the σ_κ^2 factor that intervenes in the expressions (34) and (44) is actually given by,

$$\sigma_\kappa^2 = \frac{1}{4} \int \frac{d^2\mathbf{l}}{(2\pi)^2} p_{2d}(l) W_{\theta_0}^2(l). \quad (48)$$

In practice however this approximation may not be very accurate. Even at 4.5' arcmin resolution scale (the best channels of Planck surveyor) about 20 to 25% of the primordial signal is filtered out because of the finite resolution. One problem that then should be addressed with numerical experiment is the validity of this approximation.

4. Numerical results

The numerical results are based on a series of 20 realizations of both the CMB temperature fluctuations and the displacement maps. Each map is initially 10x10 deg² large, with a pixel size of 1.17' (these are 512x512 grid maps). After regridding to take into account the lens effects and

filtering, the actual useful size is 9x9 square degrees. In Figs. 2-4 I give the averaged ellipticity distributions obtained from these 20 realizations, and the error-bars correspond to the estimated cosmic variance of one map.

4.1. The ellipticity distribution

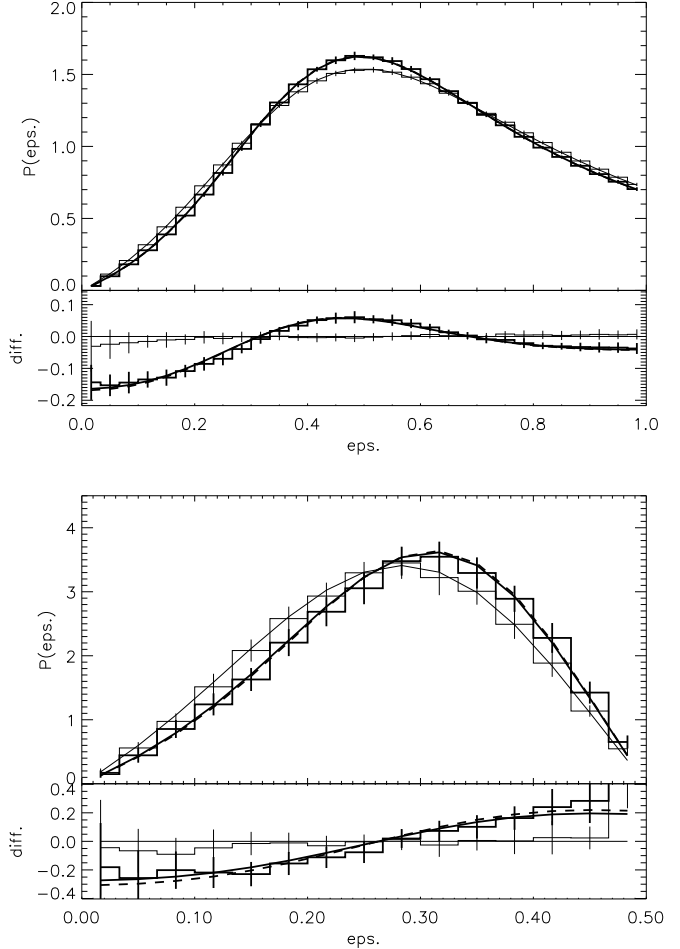


Fig. 2. The ellipticity statistics at 2.5 arcmin scale for $\sigma_8/0.6 = 2$. The statistics for the field points is given in the top panels and for the extrema points in the bottom ones. The thin lines correspond to the primordial temperature map, the thick lines to the lensed map. The error bars correspond to the cosmic variance computed for a 9x9 square degree size map. The cosmic variance has been estimated with 20 different realizations of both the primordial temperature maps and the displacement fields. The continuous lines give the theoretical predictions (34) and (44) with σ_κ given by (48). The dashed lines correspond to the best fit of the ellipticity distribution using formulae (34) or (44) where σ_κ is assumed to be a free parameter.

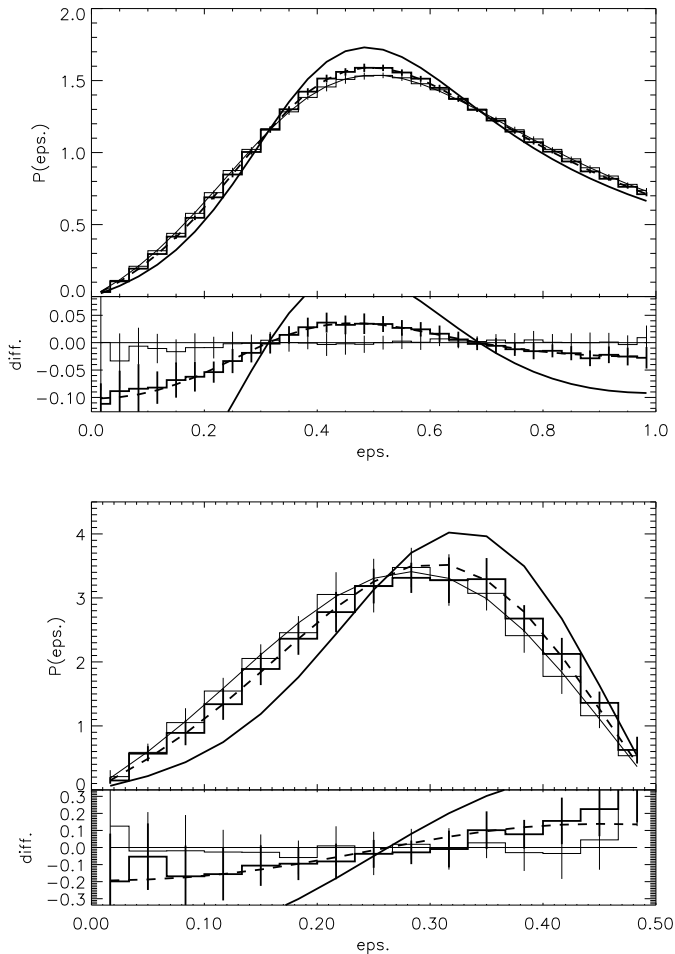


Fig. 3. Same as figure 2 with a 5 arcmin filtering scale, $\sigma_8/0.6 = 4$

The maps are filtered with a compensated filter built as the difference of two Gaussian window functions with one filtering radius being twice the other,

$$W_{\theta_0}(l) = \exp(-l^2 \theta_0^2/2) - \exp(-2l^2 \theta_0^2). \quad (49)$$

This makes the maps rather weakly sensitive to the large angular scale correlation. The correlation length of the local quantities is thus expected to be rather small, of the order of $2 \theta_0$.

The local curvature is calculated from finite differences. To be more precise the scheme which is used is the following,

$$\delta_{T,11}(i, j) = \frac{1}{3} \sum_{k=-1,1} \delta_T(i-1, j+k) - 2\delta_T(i, j+k) + \delta_T(i+1, j+k); \quad (50)$$

$$\delta_{T,12}(i, j) = \frac{1}{4} [\delta_T(i-1, j-1) - \delta_T(i-1, j+1) - \delta_T(i+1, j-1) + \delta_T(i+1, j+1)]. \quad (51)$$

where $\delta_T(i, j)$ is the local temperature fluctuations at the grid point (i, j) . The Figs 2-3 present the results of the distribution function for various filtering scales, and various normalization of the lens effects (expressed in terms of σ_8). We can see that for a very small filtering scale, 2.5 arcmin, the numerical results are in good agreement with the theoretical predictions for both the field points and the extrema.

At larger angular, the filtering effect starts to play a major role and significantly reduces the lens effects. Thus at 5 arcmin angular scale, the amplitude of the effect seems indeed to be reduced by a factor of about 2 compared to what would be expected when the smoothing effects are neglected (see table 1). This discrepancy is shown in figure 3 where the dashed lines correspond to the best fit of the lens effect when σ_κ is a free parameter. The quality of the fit shows however that the filtering effect changes the amplitude of the lens effects, but not much the e dependence of the corrective terms.

4.2. The Cosmic Variance

Because of the use of compensated filters, it is fair to assume that the a whole sky survey would simply correspond to a given number of *independent* 9×9 square degree maps. This should be particularly accurate for the local statistical indicators considered here. The cosmic variance then scales as the square root of the number of such maps. The signal to noise ratio for the lens effect is thus expected to obey the scaling property,

$$\frac{\text{Signal}}{\text{Noise}} \propto \frac{\sigma_8^2}{\sqrt{\text{Sky coverage}}}. \quad (52)$$

If one is able to get a the sky coverage of 50% as anticipated for the Planck surveyor then it means that the cosmic variance should be, for the whole survey, about 16 times less important than for a 9×9 square degree map. The signal to noise ratio is expected to be the same for a “whole” sky survey with $\sigma_8 = 0.6$ or for a 9×9 square degree map with $\sigma_8 = 4 \times 0.6$. The latter case then provides us with a realistic estimation of the Cosmic Variance for the future Planck mission.

In table 1, I summarize the results obtained for the determination of σ_κ with a best fit and the error associated with this determination. This error has been determined as the r.m.s. of the determined σ_κ^2 among the 20 realizations at my disposal. One can see that the signal ratio grows indeed with σ_8 and scales like σ_8^2 for a given filtering scale. The filtering effects however reduce the signal by a factor 3 from what would be expected with a direct determination of σ_κ . The noise is independent on σ_8 but depends slightly on the filtering scale. The signal to noise ratio expected for the Planck survey at 5' resolution scale is thus about 3 if $\sigma_8 = 0.6$.

Table 1. Values of σ_κ from direct determination with the displacement maps (eq. 48) and from best fit parameterizations. Errors give the cosmic variance for maps of 9x9 square degree size.

σ_8	ang. scale	$\sigma_\kappa^2 \times 10^3$ direct det.	$\sigma_\kappa^2 \times 10^3$, best fit, field points, no lens effects	$\sigma_\kappa^2 \times 10^3$, best fit, field points, with lens effects	$\sigma_\kappa^2 \times 10^3$, best fit, extrema, no lens effects	$\sigma_\kappa^2 \times 10^3$, best fit, extrema, with lens effects
0.6	2.5'	2.3 ± 0.1	0.2 ± 1.2	2.5 ± 1.4	0.2 ± 1.8	4.0 ± 1.7
1.2	2.5'	9.2 ± 0.3	0.2 ± 1.2	9.4 ± 1.5	1.2 ± 1.8	10.3 ± 1.8
1.2	5'	5.1 ± 0.3	0.4 ± 1.6	1.8 ± 1.6	1.0 ± 2.1	2.5 ± 2.1
2.4	5'	$20. \pm 1.$	0.4 ± 1.6	5.6 ± 1.6	1.0 ± 2.1	6.5 ± 2.2
2.4	5' + noise	$20. \pm 1.$	0.4 ± 1.5	5.6 ± 1.6	1.2 ± 2.0	6.5 ± 2.1

4.3. The effect of Noise

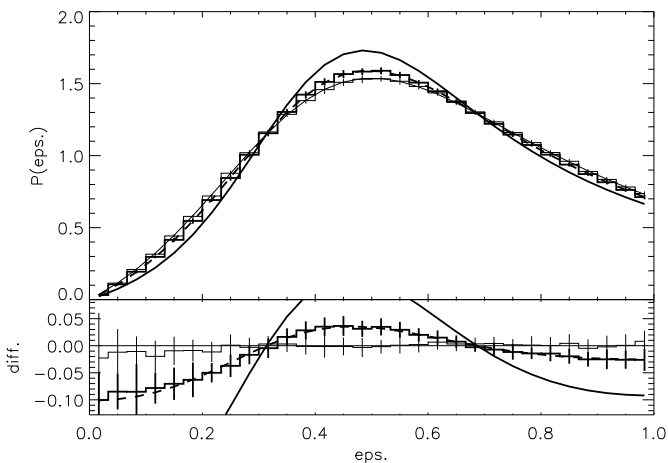


Fig. 4. Same as figure 2 with a 5 arcmin filtering scale, $\sigma_8/0.6 = 4$ and including noise

Fig. 4 and the last line of the table show the effects of noise of the measured map. Its effect is found to be very weak. However the noise here has been assumed to be a pure white noise, and thus, for the ellipticity statistics, it reproduces the Gaussian case. This is certainly not a realistic assumption. The striping introduces indeed non-local correlations that may affect significantly statistics that are related to local topological quantities. The study of the striping effect is very dependent on the experiments and is beyond the scope of this paper.

5. Discussion

5.1. The dependence on the cosmological parameters

The dependence on the cosmological parameters is explored here in a quite rough way. The temperature power spectrum, and its relation to the density power spectrum, has indeed a rather complicated dependence on all the cosmological parameters. So in this simple study I will assume that the shapes of C_l and $P(k)$ remain the same and simply discuss the dependence of the amplitude of σ_κ on the

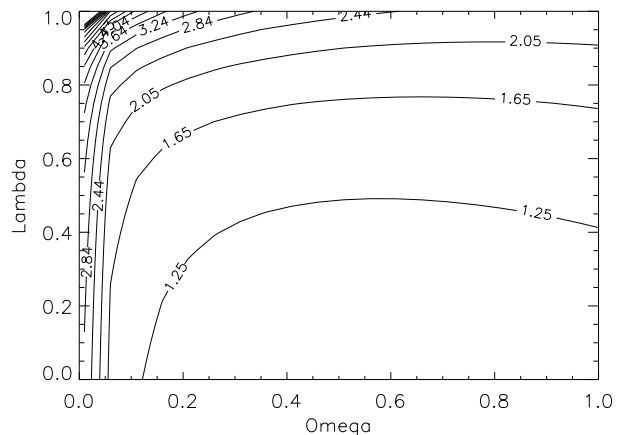


Fig. 5. The ratio $\sigma_\kappa^2(\Omega, \Lambda)\Omega^{-1}/\sigma_\kappa^2(\Omega = 1, \Lambda = 0)$ as a function of Ω and Λ for a power law spectrum with $n = -1.5$.

cosmological parameters due to the density-convergence relationship. The ratio σ_κ/σ_8 is obviously a quantity that one might want to consider but it should be compared to other constraints coming from large-scale structure formation. The number density of clusters can provide us with a constraint which is in principle free of bias contamination. It constrains the amplitude of the density fluctuations at roughly the $8 h^{-1}$ Mpc scale for an Einstein-de Sitter Universe (Oukbir et al 1997), which corresponds roughly to the scale of interest for the lens CMB effects. For open universes the dependence cannot be given simply in terms of σ_8 because linear mass scale of the galaxy clusters is shifted to a larger scale. A dependence arises then with the slope of the power spectrum (Oukbir & Blanchard 1997). Ignoring these subtleties, and following Eke, Cole & Frenk (1996) I will simply assume that the actual constraint coming from the observed number density of rich clusters can be written,

$$\sigma_8 \Omega^{0.5} \approx 0.6 \pm 0.1. \quad (53)$$

It means that the larger Ω the smaller σ_8 . To estimate the variation of σ_κ with roughly a fixed number density of clusters, one should then compute $\sigma_\kappa^2(\Omega, \Lambda)\Omega^{-1}/\sigma_\kappa^2(\Omega = 1, \Lambda = 0)$. The result is given in Fig. 5. One can see, as

expected, that the magnitude of the signal is very weakly Ω dependent if $\Lambda = 0$ but significantly grows with Λ . It implies that the signal to noise ratio would be a factor about 2 larger for a Λ -CDM.

5.2. On the interest of lens effect detection.

The observational quantities that have been investigated here have been designed to be sensitive to the non-linear couplings induced by lens effects. It is of course possible to consider other quantities, such as the Minkowski functionals, whose general properties for a Gaussian field have been recently investigated in detail (Winitzki & Kosowski 1997 and Schmalzing & Górski 1997). The lens effects might indeed significantly affect the Minkowski functional for 2D maps. For instance the shapes of high threshold peaks are shown to be more elongated, which implies that the averaged circumference near the top of the peak should increase. However, a complete theoretical investigation of this effect is quite difficult because this is a nonlocal indicator. And in general, the most efficient non-Gaussian indicators probably depend on the processes one wants to detect. The number of hot and cold spots seems to be a good way to detect topological defects. Is it obviously not the case for the lenses.

In a previous paper the four-point function was considered. Actually the local curvature can be viewed as an other way to have access to the same information. Here the four point function is simply averaged in a way that avoid too much cancellation. And other possible quantity is the collapsed four-point function, that identifies with the four order cumulant of the local temperature. This quantity however tends to cancel the contribution of the various terms. This seems not to be the case for the local curvature. It does not mean however that we cannot do better for detecting the lens effects. For instance the two-point correlation function of the local ellipticity (with orientation) might be a good indicator. However one should have in mind that the number of CMB structures per lens is rather small. It is thus not obvious that it can improve the situation.

Note that the results obtained for the lens effects, temperature four-point function or ellipticity statistics, are all sensitive to the lens two-point correlation function. It comes from the fact that the only quantity related to the lenses which is potentially available from CMB maps is its power-spectrum. The non-Gaussian properties of the lens population are for instance not accessible.

If it is actually possible to detect a lens effect, the smallness of the signal to noise ratio with which it can be determined indicates that it will be pointless to use this information as a mean to constrain the cosmological parameters. But, it would be extremely interesting to be able to check that the amount of lens effects computed from models favored by the CMB power spectrum are in agreement with its detection, or its non-detection.

Note however that other secondary effects might as well induce non-Gaussian properties. The Rees-Sciama effect in particular is due to the evolving non-linear potentials and has a source term which is intrinsically non-Gaussian. A peculiar case of this effect is the moving lens effect (Birkinshaw & Gull 1983): potential wells that move perpendicularly to the line of sight induce temperature fluctuations. This effect is quadratic with the cosmic fields (proportional to the local velocity times the gradient of the potential) and is thus intrinsically non-Gaussian. These cases are probably worth investigating. I expect however that they give a smaller non-Gaussian signal since the static lens effect is the only mechanism that couples the primary anisotropies to the line of sight potentials.

Acknowledgments

Part of this work has been initially pursued with Thibaut Marrel who is warmly thanked for it. The author is also grateful to Y. Mellier for many fruitful discussions and a careful reading of the manuscript, to U. Seljak and B. Jain for the use of their codes.

References

- Barnes, C. & Turok, N. 1997, hep-ph/9702377
- Bernardeau, F. 1997, A&A, 324, 1
- Birkinshaw, M. & Gull, S.F. 1983, Nature, 302, 315
- Blanchard, A. & Schneider, J. 1987, A&A, 184, 1
- Bond, J.R., Efstathiou, G. 1987, MNRAS, 226, 655
- Cayón, L., Martínez-González, E. & Sanz, J.L. 1993a, ApJ, 403, 471
- Cayón, L., Martínez-González, E. & Sanz, J.L. 1993b, ApJ, 413, 10
- Cole, S., Efstathiou, G. 1989, MNRAS, 239, 195
- Fukushige, T., Makino, J. & Ebisuzaki, T. 1994, ApJ, 436, L107
- Hamilton, A.J.S., Matthews, A., Kumar, P. & Lu E. 1991, ApJ, 374, 1
- Jain, B., Mo, H. J. & White, S.D.M. 1995, MNRAS, 276, L25
- Jungman, G., Kamionkowski, M., Kosowsky, A. & Spergel, D.N., 1996, astro-ph/9512139
- Kashlinsky, A. 1988, ApJ, 331, L1
- Linder, V.E., 1990, MNRAS, 243, 353
- Oukbir, J., Blanchard, A. 1997, A&A, 317, 1
- Oukbir, J., Bartlett, J.G., Blanchard, A. 1997, A&A, 320, 365
- Peacock, J.A. & dodds, S. J. 1996, MNRAS, 282, 877
- Pen, U., Spergel, D., Turok, N. 1994, Phys. Rev. D, 49, 692
- Sasaki, M. 1989, MNRAS, 240, 415
- Smoot, G. F. et al. 1993, ApJ, 396, L1
- Seljak, U. 1996, ApJ 463, 1.
- Seljak, U. & Zaldarriaga, M. 1996, ApJ, 469, 437
- Schmalzing, J. & Górski, K.M. 1997, astro-ph/9710185
- Suginohara, M., Suginohara, T., Spergel D. N. 1997, astro-ph/9705134
- Tomita, K. & Watanabe, K. 1989, Prog. Theor. Phys., 82, 563
- Turok, N. 1996, ApJ, 473, L5
- Winitzki, S. & Kosowsky, A. 1997, astro-ph/9710164

This article was processed by the author using Springer-Verlag
L^AT_EX A&A style file *L-AA* version 3.